INTERNATIONAL JOURNAL FOR NUMERICAL AND ANALYTICAL METHODS IN GEOMECHANICS
Int. J. Numer. Anal. Meth. Geomech., **23**, 1473–1492 (1999)

A STUDY ON PROBLEMS ASSOCIATED WITH FINITE ELEMENT EXCAVATION ANALYSIS BY THE STRESS-FLOW COUPLED METHOD

HIROYASU OHTSU,*[,1,†] YUZO OHNISHI,[1,‡] HARUO TAKI[2,§] AND KATSUMI KAMEMURA[2,§]

[1] *School of Civil Engineering, Kyoto University, Yosida-honmachi, Sakyou-ku, Kyoto 60601, Japan*
[2] *Civil Engineering Department, Taisei Corporation, 1-25-1 Nishi-shinjuku, Shinjuku-ku, Tokyo 16306, Japan*

SUMMARY

This study attempts to address some problems associated with excavation analysis by means of the stress-flow coupled method. This is done through the investigation of two examples, both of which are excavation analyses modelling a sequential excavation process. The first example is a three-dimensional elastic analysis of a tunnel constructed in soft rock layer. The second example is an axi-symmetric elasto-plastic analysis of a shaft constructed in slightly overconsolidated clay layer. In order to clarify the effect of sequential excavation process on the analysis results, a conventional two-dimensional analysis on each example is also carried out. Through this study, we will demonstrate that it is essential to consider in detail the incremental advance of a tunnel face when one investigates the change of pore water pressure and stresses surrounding a tunnel face during excavation. Additionally, on the basis of the analytical results obtained, a proposal is presented for evaluating the stability of rock mass surrounding a tunnel during construction. Copyright © 1999 John Wiley & Sons, Ltd.

KEY WORDS: finite element analysis; excavation; stress-flow coupled analysis; three-dimensional analysis; tunnel face effect; elasto-plastic analysis

INTRODUCTION

Japan has a limited amount of land, and efforts to make effective use of the land available have led to the conceptualization and planning of various large-scale underground structures. For examples, tunnels more than 10 m in diameter, such as the Trans-Tokyo Bay Highway Tunnel, are under construction are large cross-section tunnels that will take three-lane expressways through mountains, such as that forming part of the Second Tomei Expressway Plan, are in the planning stage.

Typical of these plans is the challenge of forming largest ever underground structures deeper below the surface than previously attempted. Thus, the design requirements for underground construction are changing, and numerous studies have been carried out from viewpoints of both design and construction.

*Correspondence to: Hiroyasu Ohtsu, School of Civil Engineering, Kyoto University, Yosida-honmachi, Sakyou-ku, Kyoto 60601, Japan. E-mail: ohtsu@geotech.kuciv.kyoto-u.ac.jp
†Doctor of Engineering, Associate Professor
‡Doctor of Engineering, Ph.D., Professor
§Master of Engineering

CCC 0363–9061/99/131473–20$17.50

Received March 1996
Revised 28 October 1996 and 14 August 1997

From a structural design point of view, the most important issue is whether the underground structure and rock mass will remain stable during excavation, and this needs to be evaluated for large-scale structures under a diverse range of geological conditions. Such analysis requires techniques that can accurately predict the behaviour of the underground structure and rock mass as excavation proceeds. The requirements to predict geomechanical behaviour more accurately have caused a gradual shift of the numerical analysis method from conventional elastic analysis toward non-linear or elasto-plastic analysis. While numerical techniques have grown in sophistication, an important question has arisen as to whether the results of these more sophisticated analytical techniques accurately reflect the physical nature of actual excavation problems.

From a mathematical viewpoint, actual excavation problems can be considered as a peculiar boundary value problem that causes a change in the three-dimensional boundary conditions due to the progress of a tunnel face. Thus, in a strict sense, excavation analysis requires a technique that takes into account three-dimensional factors such as the incremental advance of a tunnel face.

Conventionally, this need has been understood in tunnel excavation analysis, but three-dimensional behaviour has been reduced to two-dimensional analysis because of limitations imposed by computer technology and processing time. As a result of these limitations, many techniques for modelling three-dimensional effects, using simplified models in a two-dimensional condition, have been proposed. Among the conventional simplified methods, a typical one is called the characteristics curve method,[1] in which the excavation process is calculated by proportionally changing forces released by excavation, according to stresses predetermined in a two-dimensional condition. However, strictly speaking, when one adopts the simplified methods represented by the characteristics curve method, a precise evaluation of the change in stress as the tunnel face advances incrementally is impossible. For example, it is impossible to accurately evaluate meaningful changes in pore water pressure caused by the three-dimensional changes in the structural system as the tunnel face advances.

To clarify the issues mentioned above, the authors have demonstrated, using the results of axi-symmetric elastic analysis by means of a stress-flow coupled technique on a deep vertical shaft, that an effective stress path obtained by two-dimensional analysis differs completely from that obtained in an analysis that takes into account incremental advance of the tunnel face.[2] In addition, we have pointed out that, in a case where non-linear stress–strain relations dependent on the stress path are adopted in conventional two-dimensional analysis, there is a risk of obtaining analytical results that diverge completely from the original aim of the analysis (the change in effective stress due to excavation) because the effective stress paths are different.

In this study, the authors apply the stress-flow coupled technique formulated by finite element methods, to the following examples as a means to investigate problems associated with the excavation analysis mentioned above:

(1) Example 1: A three-dimensional elastic analysis of a tunnel constructed in soft rock layer
(2) Example 2: An axi-symmetric elasto-plastic analysis of a shaft constructed in slightly overconsolidated clay layer

In order to clarify the effect of sequential excavation process on the analysis results, the conventional two-dimensional analysis on each example is also carried out.

The elasto-plastic constitutive equation adopted in Example 2 is the Ohta model,[3] which is essentially equivalent to the Cam clay model,[4] since this model has generally been applied to the analysis on geotechnical structures constructed in soft clay in Japan.

Based on the results of Examples 1 and 2, we present a new proposal to evaluate the stability of the underground structure during excavation through effective stress analysis.

GOVERNING EQUATIONS

Governing equations[5] adopted in this investigation, which we derived based on Biot's two-phase mixture theory,[6] are expressed as follows:

$$\left[\frac{1}{2}D_{ijkl}(u_{k,l}+u_{l,k})+\beta\,\delta_{ij}\,\gamma_{\mathrm{w}}(\varphi+z)\right]_{,j}+\bar{\rho}_{\mathrm{s}}b_i=0$$

$$\left[k\,(\varphi+z)_{,i}\right]_{,i}=-\beta\,\frac{\partial u_{i.i}}{\partial t}+\gamma_{\mathrm{w}}\frac{1}{Q}\frac{\partial(\varphi+z)}{\partial t} \tag{1}$$

$$\bar{\rho}_{\mathrm{s}}=\rho_{\mathrm{s}}-\beta\delta_{ij}\gamma_{\mathrm{w}}\delta_{i3} \tag{2}$$

In which D_{ijkl} is the stiffness matrix; u_i is the displacement component in i-direction; δ_{ij} is Kronecher's delta; γ_{w} is the density of water; φ is pressure head; z is gravitational head; ρ_{s} is density of soil and/or rock; b_i is the body force component in i-direction; k is the coefficient of permeability.

Also parameters β, $1/Q$ in equation (1) are expressed as follows:

$$\beta=1-\frac{c_{\mathrm{s}}}{c_{\mathrm{b}}}$$

$$\frac{1}{Q}=nc_{\mathrm{b}}\left(\frac{c_l}{c_{\mathrm{b}}}\right)+(1-n)c_{\mathrm{b}}\left(\frac{c_{\mathrm{s}}}{c_{\mathrm{b}}}\right)-c_{\mathrm{s}}\left(\frac{c_{\mathrm{s}}}{c_{\mathrm{b}}}\right) \tag{3}$$

In which c_l is the compressibility of pore water; c_{s} is the compressibility of grain or particle composing soil and/or rock: c_{b} is the compressibility of rock and/or soil matrix; n is porosity.

When comparing the governing equations with the equations defined by Biot's general multi-dimensional consolidation theory,[7] we can clarify the meaning of β and $1/Q$ as a function of physical properties such as n, c_l, c_{s} and c_{b}.

The finite element formulation of equation (1) is carried out by adopting Galerkin's method.

EXAMPLE 1: A THREE-DIMENSIONAL ELASTIC ANALYSIS OF A TUNNEL CONSTRUCTED IN SOFT ROCK LAYER

The example presented in this section is a three-dimensional elastic analysis on a tunnel constructed in soft rock layer. In order to examine the effect of sequential excavation process on the analysis results, a conventional two-dimensional analysis of the tunnel is also carried out.

Analytical conditions

The basic analytical conditions of this example are summarized as follows:

(1) Stress-flow-coupled analysis is applied to both three-dimensional and two-dimensional analysis.

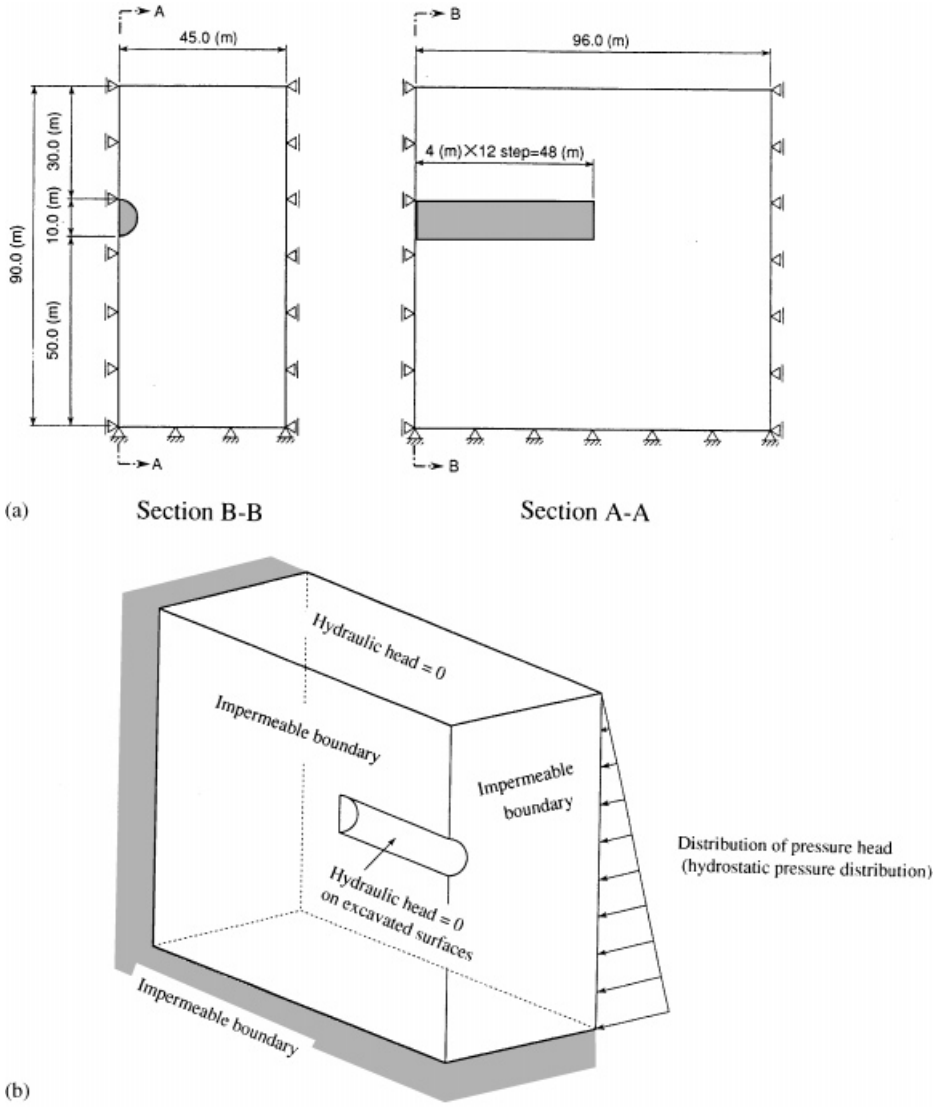

Figure 1. Three-dimensional numerical model and boundary conditions. (a) Structural model and mechanical boundary conditions; (b) Hydraulic boundary conditions

(2) The size of the tunnel related to this analysis is 10 m in diameter and 48 m in length, as shown in Figures 1 and 2, in which both mechanical boundary conditions and hydraulic boundary conditions are also described.
(3) The analytical model in the two-dimensional plane strain condition consist of a vertical cross section at a location 24 m from the portal.
(4) The analysis assumes that the tunnel is constructed in sedimentary soft rock corresponding to tertiary mud stone, and the stress–strain relationship of sedimentary soft rock is

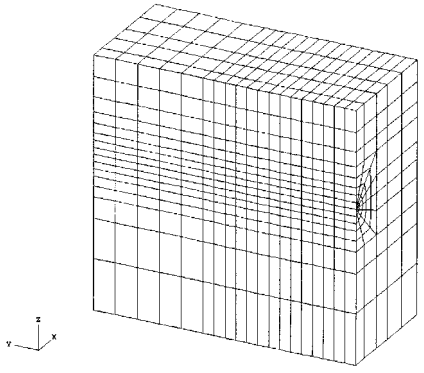

Figure 2. Three-dimensional incremental finite element mesh

Table I. Physical properties of soft rock for the analysis

Deformation coefficient, E	5000 kgf/cm^2
Poisson's ratio, v	0·33
Permiability coefficient, k	$1{\cdot}0 \times 10^{-6}$ cm/s
Lateral stress coefficient, K_0	0·8
Unit weight, γ	$2{\cdot}0 \times 10^{-3}$ kgf/cm^3
Cohesion, c'	1·0 kgf/cm^2
Angle of internal friction, φ'	25·0°

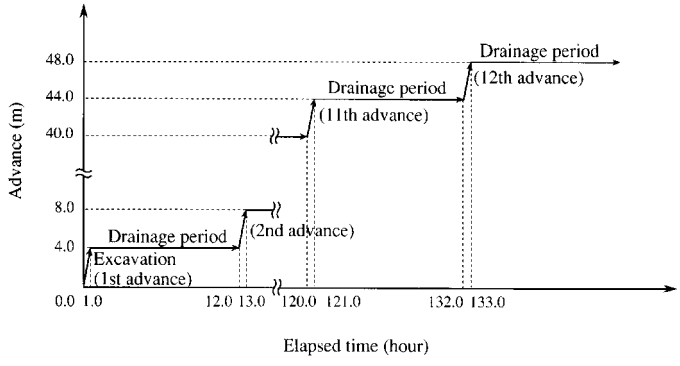

Figure 3. Modelled incremental excavation process

modelled as a linear elastic body. Also details of rock properties for the elastic analysis are shown in Table I.

(5) The incremental excavation model consists of 12 cycles, each comprising 4 m advancement followed by a 12 h drainage period, as shown in Figure 3.

(6) As regards the initial stress distribution, the effective pressure due to the overburden — with the origin at ground surface — is used to represent the initial vertical effective stress,

while this vertical effective stress value is multiplied by a lateral stress coefficient of 0·8 to model the two components of effective stress in the horizontal direction.

(7) The initial pore water pressure is assumed to follow the hydrostatic pressure distribution.

In the ordinal tunnel analysis, the effect of support members such as rock anchors or shotcrete placed in actual tunnels is generally modelled by beam elements and/or fictitious forces. Essentially, it is possible to consider the effect of support members in this analysis. However, it should be noted that the effect of any support members is not taken into account in this study, since the purpose of this analysis is to investigate the differences associated with geomechanical behaviours between the results of three-dimensional and the conventional two-dimensional analyses in detail.

Also, since the discussion in this section is based on the results obtained by the linear-elastic analysis, it is essentially impossible to check the stability of both rock mass surrounding a tunnel and a tunnel face. However, in order to cope with the limitations, the Drucker–Prager failure envelope shown in equation (4) is adopted as a means to check whether stress condition in a certain stage approaches failures due to tunnel face advancement.

$$\tau_{\mathrm{octs}} = \frac{2\sqrt{2}c' \cdot \sin\varphi'}{3 - \sin\varphi'} + \frac{2\sqrt{2}\ \sin\varphi'}{3 - \sin\varphi'}\ \sigma'_{\mathrm{m}} \tag{4}$$

where c' is a cohesion; φ' is a frictional angle.

Analytical results and discussion

Figure 4 shows the results of a three-dimensional excavation analysis. The characteristics computed are time-dependent changes in pore water pressure and stress at the crown, side walls, and base of the tunnel at a location 22 m from the portal. In discussing stress changes over time, the stress is divided into shear and volumetric (mean stress) components. The octahedral shear stress, τ_{oct}, is shown in the figure as a value representative of the shear stress component, while the mean principal stress, σ_{m}, and mean effective principal stress, σ'_{m}, are representative of the mean stress component. Points A and B in Figure 4 represent locations 2 and 6 m ahead of the prescribed tunnel cross-section, respectively.

As the figure shows, the pore water pressure begins to fall gradually as the tunnel face approaches the prescribed tunnel cross section, inching up again immediately after each advance. It falls sharply as soon as the face has passed, and then continues to drop gradually as the face recedes until the steady state is reached. The octahedral shear stress, τ_{oct}, increases gradually as the face approaches, and then increases sharply as the face passes by. Although the rate of increase slows dramatically as the face recedes, the stress does tend to increase slightly as a whole.

In contrast, the mean principal stress, σ_{m}, changes little until the instant the face is about to arrive, at which point it plunges. It fluctuates a little afterwards, and then reaches a constant value. On the other hand, the mean effective principal stress, σ'_{m}, rises sharply as the face approaches, reaches a maximum value upon arrival of the face, and declines sharply as soon as it passes. Afterwards, since the mean principal stress, σ_{m}, remains nearly constant as the face recedes, the small fall in pore water pressure resulting from drainage causes an increase in mean effective principal stress, σ'_{m}.

In order to clarify these changes in mean principal stress, σ_{m}, and mean effective principal stress, σ'_{m}, changes in the normal stress components of total stress and effective stress over time are shown in Figure 5, taking the crown of the tunnel as an example.

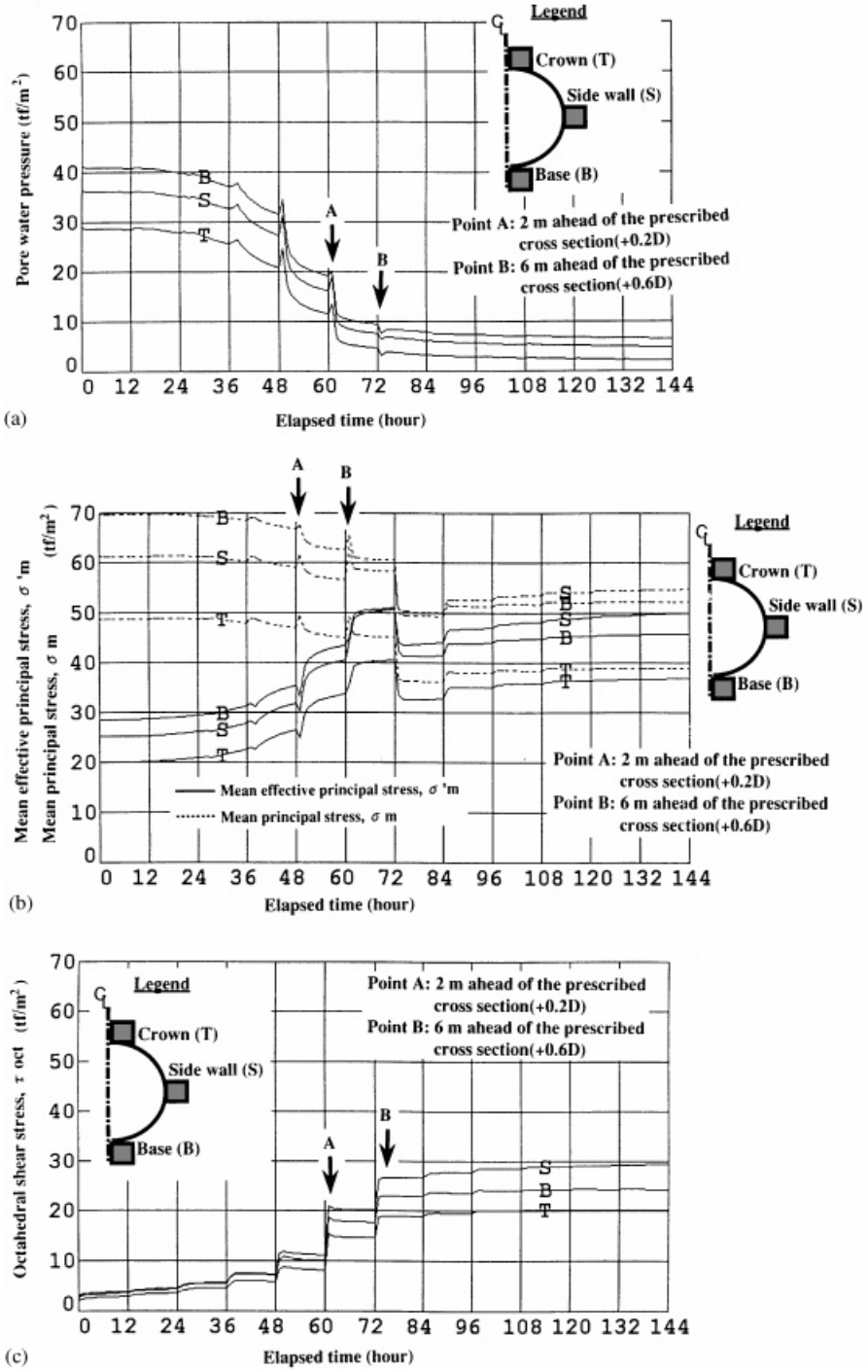

Figure 4. Results of a three-dimensional excavation analysis: changes in pore water pressure and stress with time: (a) Changes in pore water pressure with time; (b) changes in mean principal stress with time; (c) hanges in deviatoric stress with time

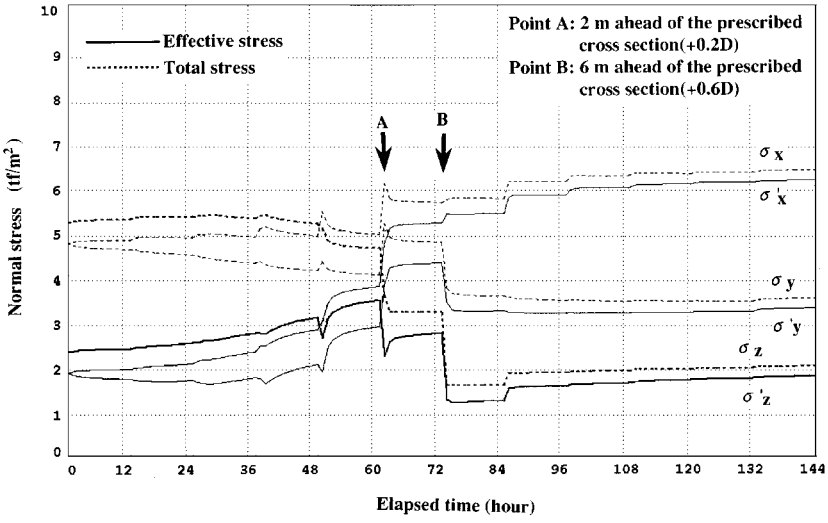

Figure 5. Changes in normal stress components of total stress and effective stress with time at the tunnel crown

First, the changes in the normal stress components of total stress indicate that the total stress in a direction perpendicular to the tunnel axis, σ_x, increases sharply soon after the face passes, but fluctuates only slightly during other operations such as drainage. The total stress in the vertical direction, σ_z, changes little until the face arrives, when it drops sharply and continues to fall as subsequent advances take place. The total stress in the axial direction, σ_y, decreases slowly before arrival of the face, because forces in this direction are released as the face approaches. As soon as the face comes into close proximity, however, it increases sharply (at a location 2 m ahead of the cross section). This is because the element under consideration when the face arrives is at a corner of the face, and at this position the axial stress increases due to the tunnel face effect. Since the pore water pressure decreases during subsequent drainage, and the tunnel face effect disappears after the face passes, the total stress in the axial direction later decreases until it reaches a constant value.

Accordingly, a stress component perpendicular to the tunnel wall decreases sharply soon after the face arrives and continues to fall as subsequent excavation processes take place. A stress component tangential to the tunnel wall surface sees one sharp increase immediately after the face arrives.

This discussion of the changes in normal stress components demonstrates that the temporary increase in mean principle stress, σ_{m}, just after the face passes (as shown in Figure 4) can be traced to the fact that the amount by which the total stress normal to the tunnel surface decreases is exceeded by the increase in the other normal stress components of the mean principal stress, σ_m. However, the mean principal stress tends to decrease as the pore water drops during subsequent drainage. Further, the reason for the sudden decrease in mean principal stress immediately after the subsequent excavation (at the location 6 m ahead of the cross section) is that the decrease in total stress in the axial direction, σ_y, (the total stress normal to the tunnel surface) is dominant.

We next look at the changes in normal stress components of effective stress at the tunnel crown over time, which are also shown in Figure 5. These normal stress components of effective stress tend to begin to increase gradually before the face arrives, in comparison with the total stress

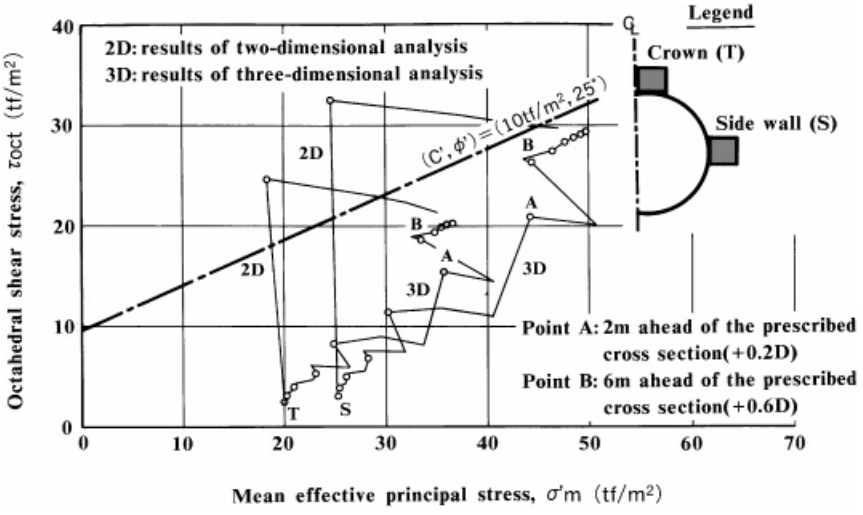

Figure 6. Comparison of stress paths as excavation advances (permeability coefficient, $k = 1{\cdot}0 \times 10^{-6}$ cm/s.)

components, because the pore water pressure drops as the face approaches. Of the normal stress components, the component normal to the tunnel surface drops sharply, as in the case of total stress, immediately after the face arrives and as subsequent advances take place. On the other hand, the component tangential to the tunnel surface increases sharply as soon as the face arrives. In contrast to the case of total stress, the axial component of effective stress, σ'_y, increases gradually as the face approaches, then increase sharply just after the face passes (at the location 2 m ahead of the cross section) because of the tunnel face effect. Afterwards, σ'_y drops sharply because the tunnel face effect disappears.

This discussion of the changes in normal stress components of effective stress indicates that the reason for the temporary increase in mean effective principal stress, σ'_m, immediately after the face pass (as seen in Figure 4) is that the fall in effective stress normal to the tunnel surface is exceeded by the increase in the other normal components of mean effective principal stress, σ'_m. After subsequent drainage, σ'_m tends to increase slightly because the decrease in pore water pressure exceeds the decrease in mean effective principal stress, σ'_m. Further, the reason for the sudden decrease in σ'_m immediately after the subsequent excavation (at the location 6 m ahead) is that decrease in axial effective stress, σ'_y, and normal effective stress is dominant.

This discussion has been limited to stresses in the vicinity of the tunnel wall. The stress patterns indicated in Figures 4 and 5 represent the most prominent changes under these pseudo-drainage conditions. Changes in stress further away from the tunnel wall are smaller and slower than those given in Figure 4, with a time lag based on the relationship between distance from the tunnel wall and drainage performance, and on the three-dimensional characteristics of stress transfer.

The next step is to reveal the problems with analysis in a two-dimensional plane strain condition by comparing the stress paths at the tunnel crown and side wall obtained in two-dimensional and three-dimensional analyses. Results for a location 22 m inside the tunnel portal are shown in Figure 6. The effective stress path obtained in a two-dimensional strain condition differs completely from the three-dimensional case. Comparing the effective stress paths shown in the figure with the Drucker–Prager failure envelope on this stress plane clarifies certain

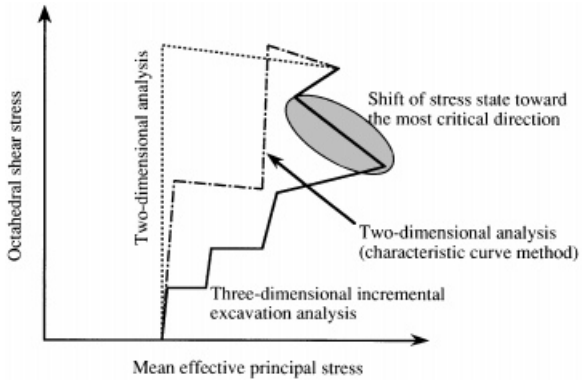

Figure 7. Comparison of effective stress paths as excavation advances (schematic diagram)

differences: the most critical stress state arises soon after an excavation step in a two-dimensional strain condition, but it occurs in the steady state after an excavation in the three-dimensional condition. That is to say, in comparison with a three-dimensional incremental excavation in a three-dimensional condition, the analytical results for a two-dimensional condition, overestimate the octahedral shear stress, τ_{oct}, immediately after an excavation step, thus giving a stress path that diverges significantly from reality.

The two-dimensional analysis results shown in Figure 6 were obtained using a technique that does not take into account tunnel face advancement. Accordingly, effective stress paths are estimated using a characteristic curve method usually adopted in two-dimensional analysis. In the characteristic curve method, a predetermined initial stress acts on a two-dimensional tunnel shape in several steps, with a constant percentage of the stress component incremented in each step. As shown in the schematic diagram in Figure 7, use of this characteristic curve method makes it possible to model the increase in octahedral shear stress, τ_{oct}, and mean effective principal stress, σ'_m, along the effective stress path in a step-wise manner, thus minimizing the differences in effective stress paths calculated in the two- and three-dimensional conditions. However, these several steps of force release in the characteristic curve method are not calculated from actual changes in the stress state that take into account the drainage after each excavation step until the tunnel face arrives. Further, the three-dimensional effects of the face during its passage across the cross section are not taken into account. Consequently, as also indicated in Figure 7, it is impossible for two-dimensional analysis based on the characteristic curve method to model the tendency of the effective stress path to become critical in the upper-left direction; that is, to suddenly approach the failure condition.

As remarked in discussing Figure 4, significant changes in stress at the tunnel wall tend to be smaller and somewhat delayed at locations more distant from the tunnel face. The behaviour at such points depends on the relationship between separation from the tunnel wall and drainage performance as well as on the three-dimensional characteristics of stress transfer. In consequence, this tendency for the effective stress path to suddenly become critical — that is, to approach the failure condition — is most pronounced close to the tunnel wall, while it is less definite at points further away because the stress changes are smaller.

This tendency to suddenly reach the critical state results from the sudden fall in mean effective principle stress, σ'_m, soon after the face passes and so it commonly arises at points close to the

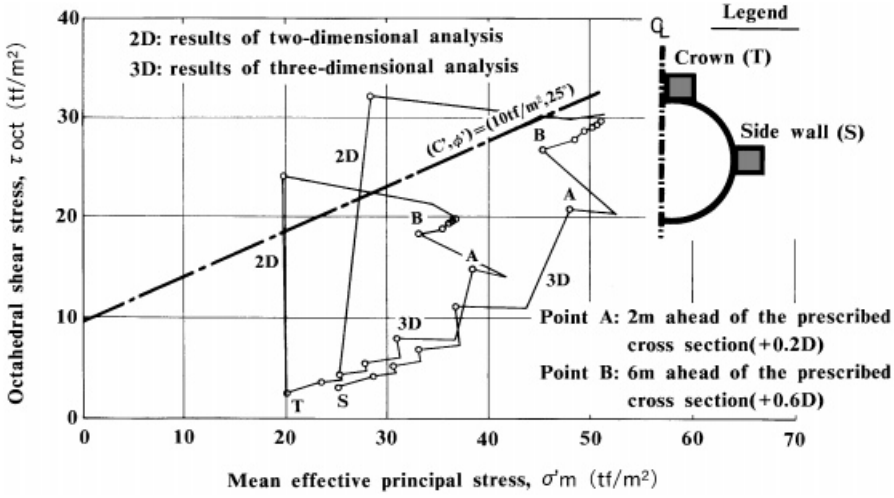

Figure 8. Comparison of stress paths as excavation advances (permeability coefficient, $k = 2{\cdot}0 \times 10^{-5}$ cm/s.)

tunnel wall. Such a change may also appear at a point close to the tunnel face irrespective of overburden pressure. This danger of suddenly approaching the failure condition is the most important issue in evaluating the stability of tunnel walls.

If the characteristic curve method is to be effectively applied to stress analysis, the conventional method based on tunnel closure must be replaced by a new characteristic curve method that also takes into account the pore water pressure as the tunnel face advances. This is because the forces released by excavation must be calculated according to the total stress, which is obtained by adding the pore pressure to the effective stress of elements to be excavated.

In order to demonstrate that changes in pore water pressure and effective stress from the initial conditions (prior to arrival of the tunnel face) depend on the permeability of the rock, stress paths obtained from two-dimensional and three-dimensional stress-flow coupled analyses are shown in Figure 8. The permeability coefficient used here is 20 times greater than that used in the earlier analysis. A comparison of these stress paths with those in Figure 6 shows that the changes in pore water pressure and effective stress prior to tunnel face arrival as seen in three-dimensional analysis now appear clearly as soon as the first excavation begins. There are distinct differences from the results of two-dimensional analysis. This clearly demonstrates that the changes in pore water pressure and effective stress before the tunnel face arrives vary greatly according to the permeability of the rock and the speed of construction (advance rate).

To further clarify this situation, the characteristic curves of internal spatial deformation and pore water pressure at a location 22 m from the portal for two different permeability coefficients are shown in Figure 9. It is evident that the greater the permeability the more the characteristic curves of the tunnel closure and the pore water pressure, diverge. At high permeability, the change in the characteristic curve of the pore water pressure in dominant until the tunnel face arrives.

These results make it obvious that, in order to approximate the advancement of a tunnel face, separate characteristic curves of effective stress and pore water pressure respectively, must be established. One critical issue to be considered in using the pore water pressure characteristic curve, and in treating pore water pressure as a force that is released incrementally by excavation, is how to establish the water drainage conditions for the tunnel walls before the tunnel face arrives.

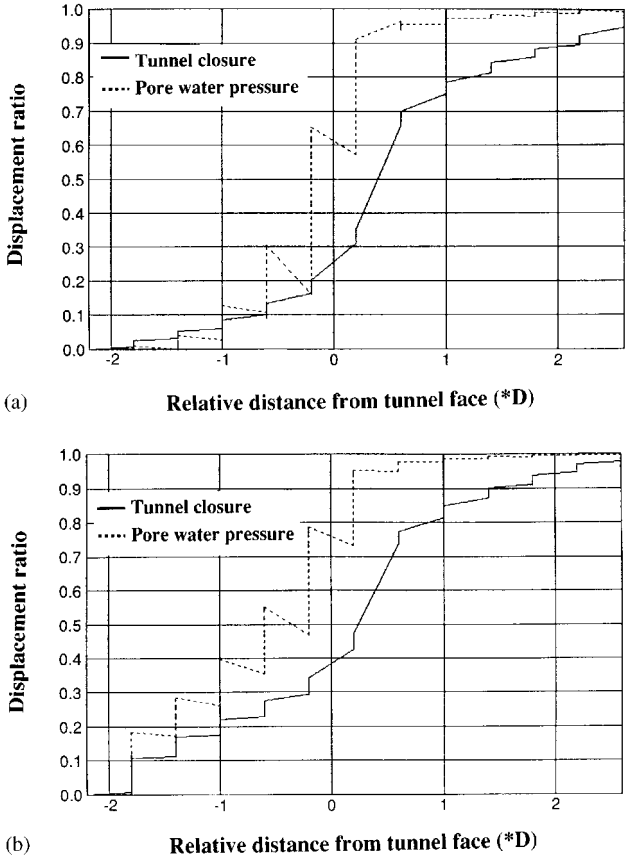

Figure 9. Comparison of characteristic curves of tunnel closure and pore water pressure: (a) Permeability cofficient, $k = 1{\cdot}0 \times 10^{-6}$ cm/s; (b) Permeability coefficient, $k = 2{\cdot}0 \times 10^{-5}$ cm/s

This discussion makes it very clear that effective stress paths obtained from excavation analysis in a two-dimensional plane strain condition diverge from the actual situation, although from a design perspective they give results on the safe side. When using stress-flow coupled analysis in excavation problems and adopting non-linear constitutive equations for stress–strain relationships, it is necessary to carry out the analysis taking into account the incremental excavation in an axi-symmetric or a three-dimensional condition.

A comparison of the effective stress paths given in Figures 6 and 8 shows that the stresses in the final steady state obtained from analysis in a two-dimensional strain condition agree approximately with those obtained from analysis in a three-dimensional condition. Furthermore, the results of three-dimensional analysis taking into account incremental excavation indicate that, judging from existing failure criteria, the most critical stress state arises in the final steady state after excavation. This appears to hold true in general, since the changes in mean principal stress become less significant as the overburden increases, whereas the octahedral shear-stress increases become more significant as excavation advances. We can thus conclude that it is possible to simplify design by simply evaluating the final steady state if the rock matrix is assumed to be linear elastic.

EXAMPLE 2: AN AXI-SYMMETRIC ELASTO-PLASTIC ANALYSIS OF A VERTICAL SHAFT CONSTRUCTED IN SLIGHTLY OVERCONSOLIDATED CLAY LAYER

The effective stress paths obtained from three-dimensional analysis in Example 1 are similar to those obtained by the authors in the elastic analysis of a deep vertical shaft in an axi-symmetric condition[2]; they differ totally from those obtained in two-dimensional analysis. In order to clarify the problems associated with using non-linear constitutive equations in excavation analysis, we now look into the differences between effective stress paths obtained from two-dimensional analysis based on an elasto-plastic constitutive equation and those obtained from axi-symmetric analysis, taking into account a sequential excavation process.

The example adopted in this section is an axi-symmetric elasto-plastic analysis of a vertical shaft constructed in slightly overconsolidated clay layer. In order to clarify the effect of sequential excavation process on the analysis results, conventional two-dimensional analysis on each example is also carried out.

Analytical conditions

The basic analytical conditions of this example are summarized as follows:

(1) Stress-flow coupled analysis is applied to both axi-symmetric and two-dimensional analysis.
(2) The size of the vertical shaft related to this analysis is 2 m in diameter and 20 m in depth, as shown in Figure 10, in which both mechanical boundary conditions and hydraulic boundary conditions are described.

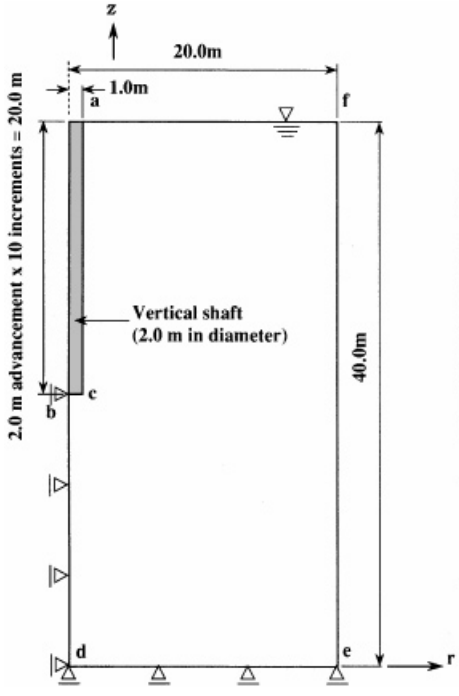

Boundary conditions		
	Mechanical boundary conditions	Hydraulic boundary conditions
ac	—	$\psi=0$
bc	—	$\psi=0$
bd	$u_r=0$	$Q=0$
de	$u_z=0$	$Q=0$
ef	—	$h=40.0$
af	—	$h=40.0$

u : displacement Q : flow rate
h : total water head
ψ : pressure head

Figure 10. Analytical model and boundary conditions

Table II. Physical properties of slightly overconsolidated clay in the analysis

Comparison index, λ	0·25
Swelling index, k	0·03
Poisson's ratio, v	0·33
Unit weight, γ	$2{\cdot}0 \times 10^{-3}$ kgf/cm^3
Dilatancy coefficient, μ	0·194
Overconsolidation ratio, O.C.R.	1·1
Initial void ratio, e_0	1·0
Lateral stress coefficient, k_0	1·0
Permeability coefficient, k	$1{\cdot}0 \times 10^{-6}$ cm/s
Inclination of critical state line, M	0·567

(3) The analytical model in the two-dimensional plane strain condition consists of a horizontal cross section at a depth of 9·5 m.
(4) The analysis assumes that the vertical shaft is constructed in slightly overconsolidated clay layer, and that the Ohta model,[7] which is capable of evaluating the non-linear behaviour and dilatant characteristics of soft clay, is applied as the elasto-plastic constitutive equation. Also, details of physical properties for the Ohta model are shown in Table II.
(5) The excavation advancement process is set up as follows: an advance of 2 m per cycle over a period of one day followed by an 11-day standby to allow water to drain; 10 cycles are taken to reach a final shaft bottom at a depth of 20 m.
(6) As for the initial stress distribution, the effective pressure due to the overburden — with the origin at ground surface — is used to represent the initial vertical effective stress. It is assumed that the two components of effective stress in the horizontal direction are equal to this vertical effective stress value.
(7) The initial pore water pressure is assumed to follow the hydrostatic pressure distribution, which is equivalent to the constant total head boundary as shown in Figure 10.

Also, it is assumed that the effect of support members such as rock anchors or shotcrete is not taken into account in this study for the same reason as that mentioned in Example 1.

Stress–strain relationship based on the Ohta model[8]

(a) Elastic stress–strain relation

Based on the relationship between void ratio e and consolidated pressure σ'_m in overconsolidated state, the non-linear elastic moduli (Lame's constants) $\tilde{\lambda}$ and $\tilde{\mu}$ are obtained as follows:

$$\tilde{\lambda} = \frac{1+e}{\kappa}\,\sigma'_m - \frac{2}{3}\,\tilde{\mu}$$

$$\tilde{\mu} = \frac{3\ (1-2v)}{2\ (1+v)}\,\frac{1-e}{\kappa}\,\sigma'_m \tag{5}$$

where κ is swelling index; v is Poisson's ratio.

(b) Elasto-plastic stress–strain relation

When one adopts the Ohta model as the elasto-plastic constitutive equation, the yield function is expressed as follows:

$$f(\sigma'_{ij},\, p) = \frac{\tau_{\mathrm{oct}}}{\sigma'_{\mathrm{m}}} + \frac{\lambda - \kappa}{(1 + e_0)\mu} \ln \frac{\sigma'_{\mathrm{m}}}{p} \tag{6}$$

in which λ is the compression index; e_0 is the initial void ratio; μ is the dilatancy coefficient; p is the hardening parameter.

Considering the failure condition, which is equivalent to critical state, defined by equation (6), we can obtain the following relation:

$$\tau_{\mathrm{oct}} = \frac{\lambda - \kappa}{(1 + e_0)\mu}\, \sigma'_{\mathrm{m}} \tag{7}$$

When one compares the Ohta model with the Cam clay model, the feature of the Ohta model is that the inclination of critical state line M can be expressed by the following function of physical properties:

$$M = \frac{\lambda - \kappa}{(1 + e_0)\mu} \tag{8}$$

When one takes the total differential of the yield function expressed by equation (6) with stress σ'_{ij} and the hardening parameter p, the equation that relates both the incremental stress $\mathrm{d}\sigma'_{ij}$ and the incremental plastic strain $\mathrm{d}\varepsilon^{\mathrm{p}}_{ij}$ is derived as follows:

$$\mathrm{d}f = \frac{\partial f}{\partial \sigma'_{\mathrm{m}}}\, \mathrm{d}\sigma'_{ij} + \frac{\partial f}{\partial p}\, \frac{\partial p}{\partial \varepsilon^{\mathrm{p}}_{ij}}\, \mathrm{d}\varepsilon^{\mathrm{p}}_{ij} \tag{9}$$

Based on the associated flow rule and the normality rule, the incremental elasto-plastic stress–strain relations are derived as follows:

$$\mathrm{d}\sigma'_{ij} = D^{\mathrm{ep}}_{ijkl}\, \mathrm{d}\varepsilon_{kl} \tag{10}$$

where

$$D^{\mathrm{ep}}_{ijkl} = D^{\mathrm{e}}_{ijkl} - \frac{D^{\mathrm{e}}_{ijmn}\, (\partial f / \partial \sigma'_{mn})\, (\partial f / \partial \sigma'_{pq})\, D^{\mathrm{e}}_{pqkl}}{(\partial f / \partial \sigma'_{mn})\, D^{\mathrm{e}}_{mnpq}\, (\partial f / \partial \sigma'_{pq}) - (\partial f / \partial p)\, (\partial p / \partial \varepsilon^{\mathrm{p}}_{mn})\, (\partial f / \partial \sigma'_{mn})} \tag{11}$$

Also, the component of stiffness matrix is expressed as follows:

$$[D^{\mathrm{ep}}_{ijkl}] = \begin{bmatrix} \tilde{\lambda} + 2\tilde{\mu} & \tilde{\lambda} & \tilde{\lambda} & 0 \\ \tilde{\lambda} & \tilde{\lambda} + 2\tilde{\mu} & \tilde{\lambda} & 0 \\ & & \tilde{\lambda} + 2\tilde{\mu} & 0 \\ & & & \tilde{\mu} \end{bmatrix} - \frac{1}{W} \cdot \begin{bmatrix} A^2 & A{\cdot}B & A{\cdot}C & A{\cdot}D \\ A{\cdot}B & B^2 & B{\cdot}C & B{\cdot}D \\ A{\cdot}C & B{\cdot}C & C^2 & C{\cdot}D \\ A{\cdot}D & B{\cdot}D & C{\cdot}D & D^2 \end{bmatrix} \tag{12}$$

In which the notations shown in equation (12) are as follows:

$$f_{ij} = \frac{\partial f}{\partial \sigma'_{ij}}$$

$$W = \tilde{\lambda} f^2_{mm} + 2\tilde{\mu} f_{mn} f_{mn} - \frac{\partial f}{\partial p}\, \frac{\partial p}{\partial \varepsilon^{\mathrm{p}}_{kl}} f_{kl}$$

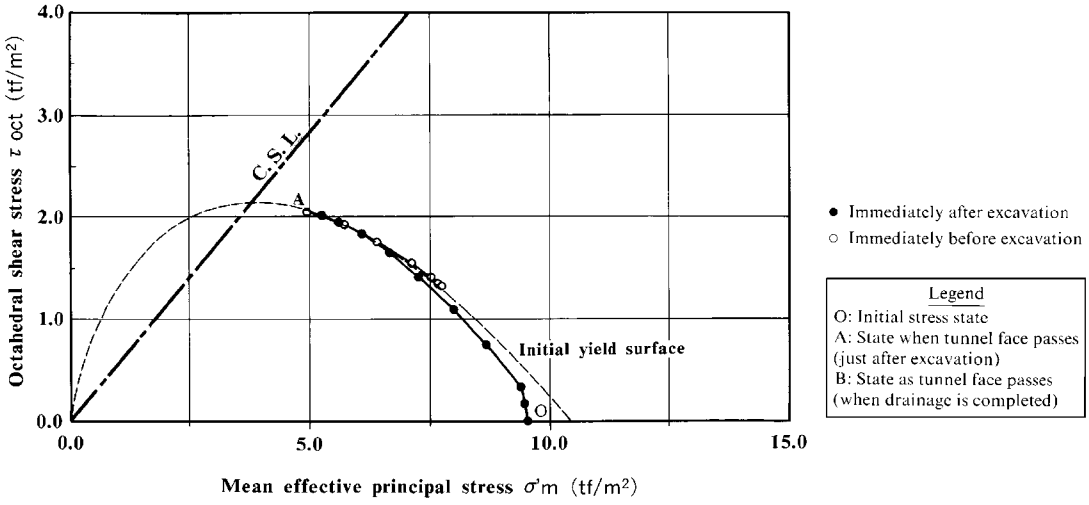

Figure 11. Effective stress paths for vertical shaft walls (results of two-dimensional analysis)

$$A = \tilde{\lambda} f_{mm} + 2\tilde{\mu} f_{11}$$
$$B = \tilde{\lambda} f_{mm} + 2\tilde{\mu} f_{12}$$
$$C = \tilde{\lambda} f_{mm} + 2\tilde{\mu} f_{33}$$
$$D = 2\tilde{\mu} f_{12}$$

Analytical results and discussion

Figure 11 shows the effective stress path for a vertical shaft wall element at a depth of 9·5 m obtained from analysis in the two-dimensional plane strain condition with the elasto-plastic model. It is clear that when an elasto-plastic constitutive model is adopted for the excavation problem, the effective stress path differs considerably from the path obtained using the linear elastic model, which was shown in Figure 6.

The stress path shown in Figure 11 can be described as follows:

(1) The stress path during an excavation phase calculated in a pseudo-undrained condition moves from Point O, which represents initial stress state, to Point A along the undrained path determined by initial stress state. Since negative dilatancy characteristics are prominent during this phase, the mean effective principal stress, σ'_{m}, decreases and the octahedral shear stress, τ_{oct}, increases.
(2) The stress path during the drainage moves from Point A to Point B on the boundary state surface. Since the dissipation of pore water pressure due to drainage is prominent, the mean effective principal stress, σ'_{m}, increases and the octahedral shear stress, τ_{oct}, decreases.
(3) Therefore, this two-dimensional analysis shown that the most critical stress state arises immediately after an excavation.

Figure 12 shows the stress path for a vertical shaft wall element at a depth of 9·5 m obtained from analysis in the axi-symmetric condition. The path is utterly different from that in Figure 11.

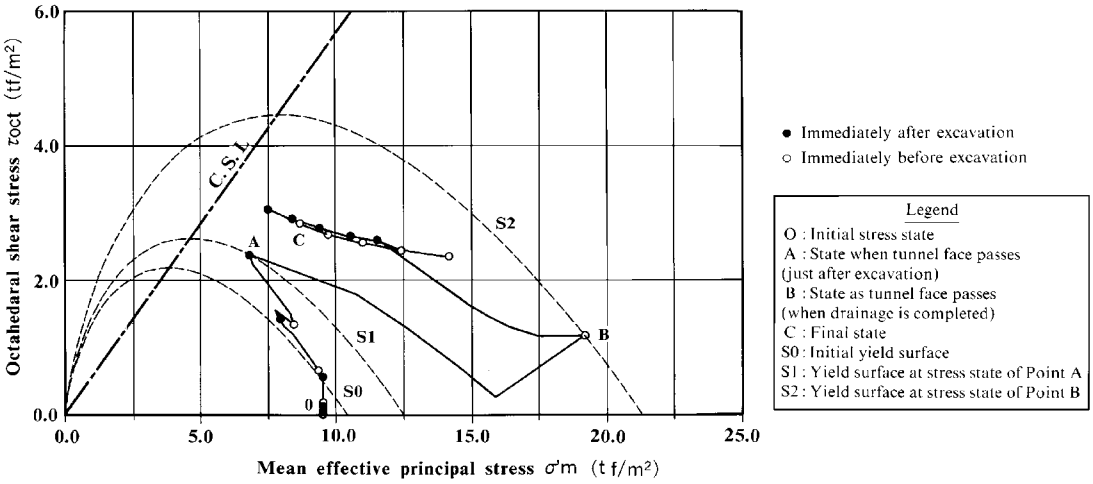

Figure 12. Effective stress paths for vertical shaft walls (results of axi-symmetric sequential analysis)

The stress path shown in Figure 12 can be described as follows:

(1) The stress path moves from Point O, which represents initial stress state, to Point A, which is located on the boundary surface in the vicinity of the initial yield surface, S_0, until the shaft face arrives.
(2) During the drainage after the face passes, the stress path moves on the boundary surface from Point A to Point B, which is located on another yield surface S_2. Since the dissipation of pore water pressure due to drainage is prominent, an increase in the mean effective principal stress, σ'_m, is noteworthy as compared with the two-dimensional results.
(3) During subsequent excavations, the mean effective principal stress, σ'_m, increases and decreases repeatedly in response to the cyclic excavation and drainage process, finally settling down to a steady state.

In this situation where the incremental excavation is taken into account, the most critical stress state arises immediately after the face passes, as marked by Point A in Figure 12. This corresponds to the analysis in the two-dimensional plane strain condition. However, as the stress path moves to the final steady state from Point B during the drainage, the stress state moves within the yield surface determined by the stress state at Point B. Accordingly, the stress state moves from the elasto-plastic domain into a non-linear elastic domain. That is to say, no failure can occur until the effective stress path returns once again to the yield surface and the critical state is approached. Therefore, it is impossible to discuss failures on the basis of the final state obtained in this analysis. The shift from the elasto-plastic domain to the elastic domain is caused by adopting an elasto-plastic constitutive equation of the isotropic hardening type, the Ohta model[3] in this case.

Fundamentally, the use of elasto-plastic constitutive equations of the isotropic hardening type is applicable only when they are applied to problems such as earth filling and load bearing capacity, where external forces are responsible for imposing the loading. This means there is still room for considerable investigation of the applicability of isotropic hardening equations such as the Ohta model to excavation situations. This issue is common to the application of the Cam clay

model[4] (which is essentially equivalent to the Ohta model) and the Sekiguchi–Ohta model[9] (improved Ohta model), in cases where external forces act to release loads.

The application of an elasto-plastic constitutive equation to tunnel excavation problems in an two-dimensional condition and in an axi-symmetric condition, where the incremental excavation process is taken into account, has indicated significant differences between the effective stress paths obtained. In practical construction work, it is common for two-dimensional analysis to be used. In such cases, there is considerable risk that the effective stress paths obtained when elasto-plastic constitutive equations are adopted will be quite different from the real situation. There is a need to fully understand the factors controlling this phenomenon, model them appropriately, and select suitable equations in performing excavation analysis based on effective stress.

PROPOSED SIMPLIFIED DESIGN PROCESS FOR EXCAVATION ANALYSIS

The analysis of the tunnel excavation problem discussed in Example 1 indicates that the ultimate steady state reached along the effective stress path in a two-dimensional plane strain condition agrees with that in a three-dimensional condition. Further, the three-dimensional analysis clarified that, according to existing failure criteria, the most critical state of stress is reached in the final steady state after an incremental excavation.

Based on this information, we propose a simplified procedure for evaluating the stability of underground structures, as given in Figure 13. The basic idea behind this procedure is that attention is focused solely on the steady stress state, which is the most critical state, and the non-steady behaviour during excavation is not investigated. The procedure is as follows:

(1) Firstly, the seepage force obtained from the results of steady seepage flows analysis is substituted into an equilibrium equation as a body force.
(2) The results of this analysis then form the basis for a study of the underground structure's stability using the concept of effective stress.
(3) If this indicates that there are no problems as regards stability in the steady state, the study is concluded. If, on the other hand, a problem is indicated, it is necessary to develop countermeasures by implementing an analysis that takes into account the incremental advance of the tunnel face using a stress-flow coupled analytical technique in an axi-symmetric condition or a three-dimensional condition.

A simplified procedure similar to the one mentioned above has been proposed by many researchers in order to avoid a more complicated coupled analysis. However, since the proposal shown in this paper is to determine in which situation the coupled analysis is to be adapted systematically, the aim is completely different from the proposed previously.

In recent years, non-linear constitutive equations are often applied to the evaluation of underground structure stability. In such cases, too, it is necessary to carry out an analysis that takes into account the sequential advance of the tunnel using a stress-flow coupled analytical technique in an axi-symmetric condition or a three-dimensional condition.

CONCLUSION

In this study, we have discussed various issues related to the analysis of excavations based on the concept of effective stress. Our findings can be summarized as follows:

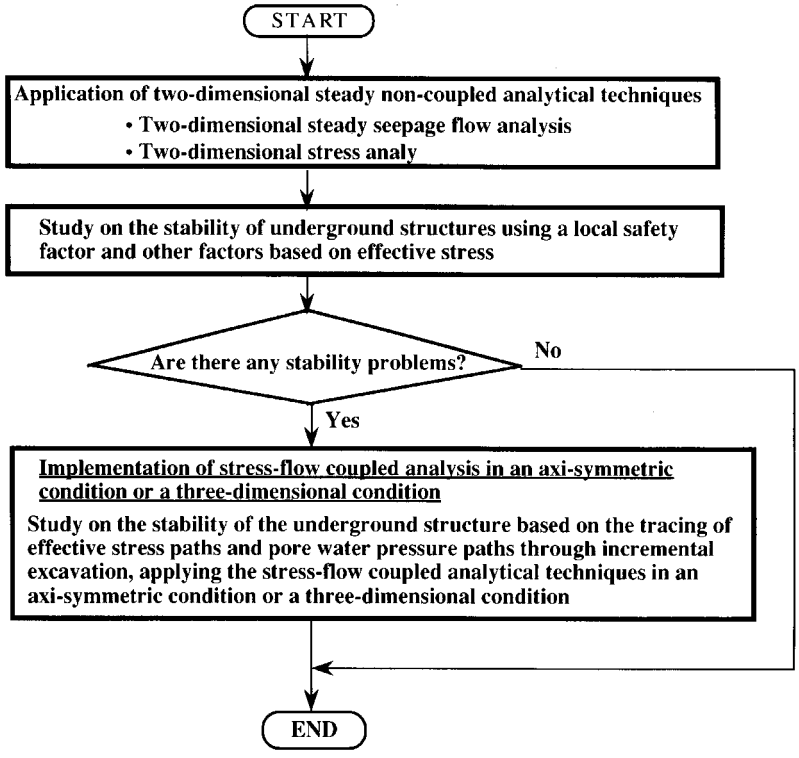

Figure 13. Simplified design procedure for excavation problems

(1) The effective stress path obtained from analysis in a two-dimensional plane strain condition differs from that in a three-dimensional condition since the pore water pressure and effective stress vary from the initial conditions by the time the tunnel face arrives. If two-dimensional effective stress analysis using a characteristic curve method is applied, it is possible to enhance the approximation and bring it close to the results of three-dimensional analysis; however, it is impossible to trace the effective stress path due to incremental excavation in detail.

(2) Since the change in pore water pressure and effective stress from the initial conditions depends greatly on the permeability of the rock and the rate of construction (advance rate), the characteristic curves for tunnel closure and pore water pressure are generally different. For these reasons, it is impossible to uniquely determine the characteristic curves for effective stress analysis. Consequently, in the detailed study of the behaviour of the bedrock and underground structure during excavation using effective stress analysis, it is absolutely essential to take into account the effects of the incremental advance of the tunnel face on the analysis results.

(3) When the ground is a linear elastic body, then — irrespective of differences in permeability — the final steady state obtained in the two-dimensional analysis agrees roughly with that in three-dimensional analysis. Referring to failure criteria, it is clear that this final state is most critical. We therefore propose simplified technique for evaluating the stability of

underground structures. This is a non-coupled steady analytical technique in which attention is focused solely on the steady and final stress state and in which a seepage force calculated from the results of steady seepage flow analysis is substituted into an equilibrium equation as a body force.

(4) There is an increasing number of cases in which non-linear constitutive equations are being applied to the evaluation of the stability of underground structures. Where such stability calculations are based on the concept of effective stress, the analysis should be performed in consideration of the incremental advance of the tunnel face, using a stress-seepage-coupled analytical technique in an axi-symmetric condition or a three-dimensional condition. Additionally, when such analysis is done, as discussed in example 2, the important point to note is that there is a limitation on the applicability of the simpler elasto-plastic analysis to excavation problems.

The authors would like to acknowledge Prof. Adachi at Kyoto University, for his continuing insightful guidance and advice related to this work.

REFERENCES

1. K. Kamemura, I. Hirano, N. Takeda and M. Sato, 'Analysis of tunnels taking into account face advancement and applications', *Proc. 27th Soil Mechanics Symp.* 1982, pp. 55–60.
2. H. Ohtsu, H. Taki and K. Kamemura, 'A study on the evaluation of groundwater flow characteristics by the excavation of a cave in sedimentary soft rock', *Proc. 24th Soil Mech. Symp.* 1992, pp. 76–80.
3. H. Ohta and S. Hata, 'A theoretical study on the stress–strain relations for clays', *Soils Found*, **11**(3)**,** 65–90 (1971).
4. A. N. Schofield and C. P. Wroth, *Critical State Soil Mechanics*, McGraw-Hill, London, 1986.
5. H. Y. Ohtsu, Ohnishi and K. Kamemura, 'A study on the design of geotechnical engineering structures considering the interaction between volumetric strain of porous media and pore water,' *J. JSCE*, (457/III-21), 87–96 (1992).
6. M. A. Biot, Mechanics of deformation and acoustic propagation in porous media,' *J. Appl. Phys.*, **33,** 1482–1498 (1962).
7. M. A. Biot, 'General theory of three-dimensional consolidation,' *J. Appl. Phys.*, **12,** 152–164 (1941).
8. T. Y. Adachi, Mochida and T. Tamura, 'Tunneling in fully saturated soft sedimentary rocks,' *Proc. 3rd Int. Conf. on Numerical Methods in Geomechanics*, Aachen, A. A. Balkman, Rotterdam, 1979, pp. 599–610.
9. H. Ohta and H. Sekiguchi, 'Constitutive equations considering anisotropy and stress reorientation in clay', *Proc. 3rd Int. Conf. on Numerical Methods in Geomechanics*, Aachen, A. A. Balkman, Rotterdam, 1979, pp. 475–478.

